buildings

Article

Influence of Non-Constant Hygrothermal Parameters on Heat and Moisture Transfer in Rammed Earth Walls

Jiaye Tan [1], Jiahua Liang [1], Li Wan [2] and Bin Jiang [1,*]

[1] School of Civil Engineering and Architecture, Southwest University of Science and Technology, Mianyang 621010, China; tanjiaye1117@163.com (J.T.); shadyleon@163.com (J.L.)
[2] Tibet Autonomous Region Energy Research Demonstration Center, Lhasa 850015, China; xizangnengyuan@163.com
* Correspondence: binjiang@swust.edu.cn

Abstract: As environment-friendly building materials, earth materials are attracting significant attention because of their favorable hygrothermal properties. In this study, the earth materials in northwest Sichuan were tested and curves of thermal conductivity and water vapor permeability with relative humidity were obtained. The function curves and constants of the two coefficients were substituted into the verified nonstationary model of heat and moisture transfer in rammed earth walls and indoor air for calculation. The difference in the calculation results when the hygrothermal parameters are functions and constants were analyzed, and the influence of the non-constant hygrothermal parameters on the heat and moisture transfer in rammed earth walls, was obtained. The test results show that thermal conductivity is linearly related to moisture content, and water vapor permeability has a small variation in the relative humidity range of 0–60% and increases exponentially above 60%. The calculation results indicate that the non-constant hygrothermal parameters have little influence on the internal surface temperature of the rammed earth walls and Mianyang City's indoor air temperature and humidity during the summer and winter. The heat transfer on the internal surface will be underestimated by using a non-constant for the hygrothermal parameter when the moisture content of the wall is low, and vice versa. In hot-humid areas or seasons with large differences in temperature and humidity between indoors and outdoors, non-constant hygrothermal parameters have a more obvious effect on heat transfer on the internal surface of the wall. The results of this study demonstrate the necessity of parameter testing.

Keywords: earth materials; thermal conductivity; water vapor permeability; non-stationary model of heat and moisture transfer

check for updates

Citation: Tan, J.; Liang, J.; Wan, L.; Jiang, B. Influence of Non-Constant Hygrothermal Parameters on Heat and Moisture Transfer in Rammed Earth Walls. *Buildings* **2022**, *12*, 1077. https://doi.org/10.3390/buildings12081077

Academic Editors: Michele Bottarelli, Yuehong Su, Carlos Jimenez-Bescos, Jingyu Cao, Jae-Weon Jeong and Devrim Aydin

Received: 11 June 2022
Accepted: 18 July 2022
Published: 23 July 2022

1. Introduction

The rapid economic development of modern society is based on a large amount of energy consumption, leading to severe environmental issues. Therefore, sustainable development has become crucial to society. Owing to rapid urbanization, the total building area in China is increasing at a rate of over 1 billion m^2 per year [1]. Building energy consumption accounts for approximately one-third of the total social energy consumption. Studies show that 40% of the building energy consumption originated from the material preparation stage [2]. In this context, materials that can effectively reduce the energy consumption in buildings, such as earth materials, are beginning to gain attention.

Compared with modern building materials, traditionally used earth materials have various advantages, such as local availability, reusability, and low cost. They lead to sustainable development [3,4], resulting in energy conservation. In addition, earth materials have good climatic suitability. They can provide superior indoor heat comfort owing to their excellent heat storage performance. When the outdoor climate changes, the indoor thermal environment can be adjusted by absorbing and releasing heat [5]. Meanwhile, they exhibit good moisture absorption and release characteristics. With a change in the environmental relative humidity, they absorb and release water vapor from the air to regulate and stabilize the indoor environmental humidity [6,7]. Although China has a long history of using rammed earth buildings, systematic research on earth materials is lacking. Research on improving the mechanical properties of earth materials is relatively common. Sabbà, M. F et al. [8] carried out preliminary sensory and qualitative analysis of the straw iber earth material and tested its properties. In recent years, researchers have focused on studying the hygrothermal properties and parameters of earth materials. He [9] measured and analyzed the effective thermal conductivity of sand with different moisture contents using a thermal constant analyzer. Nikiforova T et al. [10] used the MIT-1 m to determine the thermal conductivity of various types of earth materials and analyzed the variation in their thermal conductivity with the moisture content. Loam has a thermal conductivity change of up to 380%, with moisture content from 0% to 40%. Jin et al. [11,12] used the thermal probe method to study the variation in thermal conductivity of the various types of earth materials with moisture content. The results show that the change rate of thermal conductivity of sand commonly used in engineering exceeds 400% (moisture content from 0% to 30%), while the change rate of clay is even higher. In [13], experiments were designed to study and analyze the relationship between the water vapor permeability and relative humidity of four materials. In [14], the water vapor permeability of different building materials at different relative humidity values was measured using the desiccant method. The integral average value of the vapor permeability coefficient of various building materials between 60% and 100% has increased by more than 1000% compared with that between 0% and 60%. In addition, to improve the hygrothermal properties of the earth materials, researchers have studied earth modification [15–17]. Giada, G et al. [18] summarized the research on the hydrothermal performance of modified earth materials with different base materials (such as inorganic soil, natural fibers, minerals or recycled aggregates, and chemical stabilizers). Various studies have shown that humidity has a significant influence on the thermal conductivity and water vapor permeability of earth materials.

In the study of heat and moisture transfer in porous media, the material hygrothermal parameters are generally assumed constant for convenience [19,20], whereas the hygrothermal parameters of the material are influenced by the changes in temperature and humidity [21–23]. Accurate calculation of the heat and moisture transfer process in the building wall is the basis for HVAC system designs and building energy consumption analysis. The cooling and heating loads formed on the wall structure are related to the heat and moisture transfer inside the wall. Ignoring the influence of temperature and humidity on the hygrothermal parameters of the wall material can lead to a lack of accuracy in the calculation of the thermal and moisture transfer process, which inevitably leads to errors in the calculation of cooling and heating loads. The literature [24] shows that moisture content has a significant impact on the heat consumption of rammed earth buildings. Therefore, in this study, earth materials from Northwest Sichuan were used as the test object to explore the variation law of its thermal conductivity and water vapor permeability under different humidity values. Simulation calculations and analyses were conducted to determine the effect of hygrothermal parameters on the hygrothermal performance of the rammed earth walls, which was simulated using commercial software with an established numerical model.

2. Testing of Hygrothermal Parameters of Earth Materials

2.1. Thermal Conductivity

2.1.1. Specimen Preparation

The chemical composition of the earth materials from Northwestern Sichuan, based on X-ray fluorescence spectrometry analysis, is presented in Table 1.

Table 1. Chemical composition of earth materials.

Compound Name	SiO_2	Al_2O_3	Fe_2O_3	K_2O	MgO	Na_2O	TiO_2	CaO	SO_3
Mass fraction (%)	71.79	17.01	5.22	1.96	0.97	0.94	0.91	0.80	0.09

The earth materials were crushed and passed through a 2 mm sieve. The treated earth materials were dried in a constant temperature blast drying oven (DGG-9140A, accuracy: ±0.1 °C) until the change in the mass was less than 0.1%, within 24 h. A precision electronic balance (JJ324BC, range: 0–320 g, accuracy: ±0.1 mg) was used to weigh the adequately dried earth materials. In accordance with the specification of the earth test [25], 13% water was added to the earth materials, mixed and stirred well, poured into a mold, and pressed into a cylinder (R = 0.078 m, L = 0.021 m) using a hydraulic press. Based on relevant specifications, Shang Jianli determined the standard value of compressive strength of the earth materials as 2.0 Mpa [26]. The density of the specimen in this experiment was 2100 kg/m^3, which meets this requirement. Finally, the pressed specimens were placed at 20 ± 1 °C and 60 ± 1% RH for 28 d of curing (shown in Figure 1). The cured specimens were used for parameter testing.

Figure 1. Rammed earth specimen.

2.1.2. Thermal Conductivity Test

The moisture content of the rammed earth specimens was controlled using the weight moisture method. The expression for the moisture content is given by Equation (1). Water, with the corresponding moisture content of 2%, 4%, 6%, 8%, 10%, 12%, and 14% in sequence, was sprayed on the surface of the specimen after curing and drying. The specimen reached its plastic limit when its moisture content reached 16%; therefore, the data recorded thereafter was not considered [24]. Then, the specimen was wrapped fully with a plastic cling film, sealed, and cured for 12 h to ensure permeation of water evenly in the specimen. Finally, a thermal conductivity tester (TC-3000E, range: 0.001–10 W/mK, accuracy: ±3%) was used to measure the thermal conductivities of the specimens (Figure 2). Each specimen was measured three times to obtain the average values, which were recorded.

$$w = \frac{m_1 - m_0}{m_0} \tag{1}$$

where w is the moisture content of the rammed earth specimen (%), m_1 is the mass of the specimen after spraying it with water (kg), and m_0 is the mass of the specimen after adequate drying (kg).

Figure 2. Determination of thermal conductivity.

2.1.3. Results

The results of the thermal conductivity tests are presented in Table 2.

Table 2. Thermal conductivity of rammed earth specimens at different moisture contents.

Moisture Content (%)	Thermal Conductivity (W/mK)
0	0.528
2	0.601
4	0.644
6	0.716
8	0.782
10	0.843
12	0.904
14	0.967

By fitting the experimental data, the functional relationship between the thermal conductivity of the earth materials and the moisture content was obtained as

$$\lambda = 0.529 + 3.126w \tag{2}$$

where λ is the thermal conductivity (W/mK).

Thermal conductivity was linearly related to moisture content, with an R^2 greater than 0.98.

2.2. Water Vapor Permeability

2.2.1. Experimental Principle

The water vapor permeability can be expressed as

$$\delta_p = \frac{g}{\nabla P_v} L = \frac{g}{P_{sat}(\varphi_1 - \varphi_2)} L \tag{3}$$

where $g = \frac{\Delta m}{A \Delta t}$ is the density of the moisture flux through the specimen (kg/m^{2}s); $\frac{\Delta m}{\Delta t}$ is the moisture flux of water vapor through the specimen (kg/s); A is the superficial area of the specimen (m^2); P_{sat} is the partial pressure of the saturated vapor (Pa); φ_1 and φ_2 are the high and low relative humidity values on both sides of the specimen, respectively (%); and L is the thickness of the specimen (m).

According to standards [27], the desiccant method was used in this experiment, and the test schematic is shown in Figure 3.

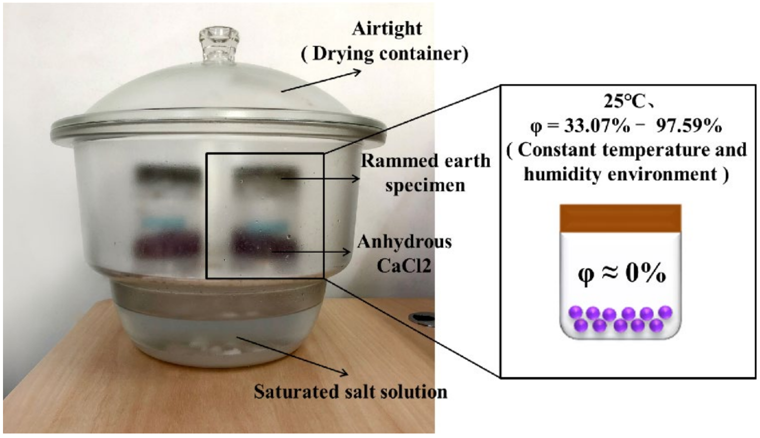

Figure 3. Schematic of the desiccant method.

2.2.2. Water Vapor Permeability Test

Twelve rammed earth specimens were prepared. Then, 50 g of anhydrous calcium chloride ($CaCl_2$) was added to each sample cup. The completely dry rammed earth specimen was placed at the mouth of the cup, sealed with beeswax, and weighed. Finally, the sample cups were placed in drying containers with different saturated salt solutions. Relative humidity values corresponding to each saturated salt solution [28] are listed in Table 3. Two sample cups were placed in each drying container as a group, and the drying container was placed in an environmental control room (temperature: 25 ± 0.5 °C, relative humidity: 60 ± 2%). The weight of the sample cups was recorded every 24 h and the variation in weight was averaged for each group of sample cups. The recording was stopped if the average variation in weight over five consecutive weights was less than 5%.

Table 3. Relative humidity corresponding to each saturated salt solution at 25 °C.

	1	2	3	4	5	6
Saturated salt solution	$MgCl_2$	K_2CO_3	NaBr	NaCl	KCl	K_2SO_4
φ (%)	33.07 ± 0.18	43.16 ± 0.33	59.14 ± 0.44	75.47 ± 0.14	84.11 ± 0.29	97.59 ± 0.53

2.2.3. Results

Data were examined through regression analysis [14] based on the curve of variation in the mass of the specimen with time at different relative humidity values obtained from the regression analysis. Equation (3) was used to calculate the water vapor permeability at six relative humidity values, and the data were fitted according to the literature [29]. The results are presented in Figure 4.

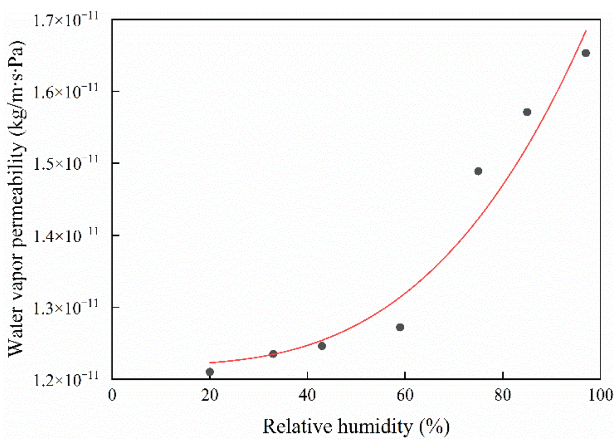

Figure 4. Fitted curve of water vapor permeability.

Figure 4 shows that the water vapor permeability changes slowly when the relative humidity is less than 60%. Meanwhile, when the relative humidity is greater than 60%, it starts to increase exponentially. From the fitted curve, the equation for water vapor permeability of earth materials was obtained as

$$\delta_p = 1.220 \times 10^{-11} + 5.114 \times 10^{-12} \varphi^{3.21} \tag{4}$$

where δ_p is the water vapor permeability (kg/m·s·Pa) and φ is the relative humidity (%).

3. Mathematical Model

The following assumptions are made when the model of heat and moisture transfer of the rammed earth wall was established [30]. The earth material was assumed to be an isotropic continuous homogeneous porous medium; the water vapor was considered as an ideal gas; the influence of gravity on moisture transfer was neglected; the moisture component inside the earth materials was only considered as a gas–liquid two-phase flow and phase change process.

3.1. Heat and Moisture Transfer Equations in the Rammed Earth Wall

3.1.1. Moisture Transfer Equation

According to [31], the total mass in the system remains the same based on Fick's and Darcy's laws, which use temperature and relative humidity as driving potentials, ignoring the velocity of airflow inside the wall. The influence of temperature inside the wall on the equilibrium moisture content of the wall material was ignored [32]. The moisture transfer equation was obtained as

$$\xi \frac{\partial \varphi}{\partial t} = \nabla \left(\left(\delta_p \varphi \frac{dP_{\mathrm{sat}}}{dT} + K_l \rho_l R_D \ln(\varphi) \right) \nabla T + \left(\delta_p P_{sat} + K_l \rho_l R_D \frac{T}{\varphi} \right) \nabla \varphi \right) \tag{5}$$

where ξ is the adsorption capacity (kg/m^3); P_{sat} is the partial pressure of the saturated vapor (Pa); K_l is the liquid water permeability (s); ρ_l is the density of liquid water (kg/m^3), and R_D is the gas constant of water vapor (J/kgK).

3.1.2. Heat Transfer Equation

The sensible heat of water vapor and liquid water and the rate of change of moisture content in the form of water vapor were ignored [33]. According to the law of conservation of energy, the heat transfer equation was obtained as

$$\left(\rho_m c_{p,m} + w c_{p,l} \right) \frac{\partial T}{\partial t} = \nabla \left(\left(\lambda + h_{lv} \delta_p \varphi \frac{dP_{sat}}{dT} \right) \nabla T + h_{lv} \delta_p P_{sat} \nabla \varphi \right) \tag{6}$$

where ρ_m is the density of building materials (kg/m^3); $c_{p,m}$ is the specific heat capacity of the dry material (J/kgK); $c_{p,l}$ is the specific heat capacity of liquid water (J/kgK), and h_{lv} is the latent heat of the water phase change (J/kg).

3.1.3. Boundary Conditions

It was assumed that the moisture exchange between the wall and the outside environment is only in the form of water vapor. The influence of solar radiation on the heat and moisture transfer on the external surface of the rammed earth wall was considered. The heat and moisture flux through the external surface of the wall can be expressed as

$$q_{n,e} = h_e \left(T_e - T_{surfe} \right) + h_{lv} g_{n,e} + \alpha q_{solar} \tag{7}$$

$$g_{n,e} = \beta_e \left(\varphi_e P_{sat,e} - \varphi_{surfe} P_{sat,surfe} \right) \tag{8}$$

The heat and moisture flux through the internal surface of the wall can be expressed as

$$q_{n,i} = h_i\left(T_i - T_{surfi}\right) + h_{lv}g_{n,i} \tag{9}$$

$$g_{n,i} = \beta_i\left(\varphi_i P_{sat,i} - \varphi_{surfi} P_{sat,surfi}\right) \tag{10}$$

where $q_{n,e}$, $q_{n,i}$ are the heat fluxes through the external and internal surfaces (W), respectively; $g_{n,e}$, $g_{n,i}$ are the moisture fluxes through the external and internal surfaces (kg/m^{2}s), respectively; h_e, h_i are the convective heat transfer coefficients of the external and internal surfaces (W/m^{2}K), respectively; β_e, β_i are the moisture exchange transfer coefficients of the external and internal surfaces (m/s), respectively; T_e, T_i are outdoor and indoor temperatures (K), respectively; T_{surfe}, T_{surfi} are the temperatures on the external and internal surfaces (K), respectively; φ_e, φ_i are outdoor and indoor relative humidity values (%), respectively; φ_{surfe}, φ_{surfi} are the relative humidity values of the external and internal surfaces (%), respectively; $P_{sat,e}$, $P_{sat,i}$ are the outdoor and indoor partial pressures of saturated vapor (Pa), respectively; $P_{sat,surfe}$, $P_{sat,surfi}$ are the partial pressures of saturated vapor on the external and internal surfaces (Pa), respectively; α is the solar absorptivity of the external surface, and q_{solar} is the solar radiation (W/m^2).

The convective heat transfer coefficients of the internal and external surfaces of the rammed earth wall were taken as 8.7 W/m^{2}K and 23 W/m^{2}K, respectively [34]. The literature [35] verified the accuracy of calculating the moisture exchange transfer coefficient of the envelope surface using the Lewis relation, as follows:

$$\beta = \frac{h}{c_{p,m}\rho_m} \tag{11}$$

where β is the moisture exchange transfer coefficient (m/s) and h is the convective heat transfer coefficient (W/m^{2}K).

3.2. Heat and Moisture Equilibrium Equation of Indoor Air in a Rammed Earth Building

To analyze the influence of moisture absorption and release on the internal surface of rammed earth walls on the indoor heat and moisture environment [30], this study established the heat and moisture equilibrium equation of indoor air in a rammed earth building.

3.2.1. Heat Equilibrium Equation of Indoor Air

The heat equilibrium equation for indoor air in a rammed-earth building can be written as

$$\rho_a c_{p,a} V \frac{\mathrm{d}T_i(t)}{\mathrm{d}t} = Q_c(t) + Q_{in}(t) + Q_v(t) + Q_s(t) + Q_L(t) \tag{12}$$

where ρ_a is the density of air (kg/m^3); $c_{p,a}$ is the specific heat capacity of air (J/kgK); V is the volume of the rammed earth building (m^3); $T_i(t)$ is the temperature of the indoor air of the rammed earth building at time t (K); $Q_c(t)$ is the convective heat exchange between the indoor air and the internal surface of the rammed earth wall at time t (W); $Q_{in}(t)$ is the heat released from the indoor equipment and personnel at time t (W); $Q_v(t)$ is the heat entering the room through ventilation at time t (W); $Q_s(t)$ is the heat obtained through windows and doors at time t (W); and $Q_L(t)$ is the latent heat owing to the moisture absorption and release from the internal surface of the rammed earth wall at time t (W).

3.2.2. Moisture Equilibrium Equation of Indoor Air

The moisture equilibrium equation for indoor air in a rammed-earth building can be written as

$$\rho_a V \frac{\mathrm{d}W_i(t)}{\mathrm{d}t} = W_V(t) + W_L(t) + W_{in}(t) \tag{13}$$

where $W_i(t)$ is the moisture content of the indoor air of the rammed earth building at time t (kg/kg); $W_V(t)$ is the moisture exchange owing to ventilation at time t (kg/s); $W_L(t)$ is the moisture exchange between the indoor air and the internal surface of the rammed earth wall at time t (kg/s); and $W_{in}(t)$ is the moisture release of indoor equipment and personnel at time t (kg/s).

3.3. Model Validation

A newly built half-year-old rammed-earth building was used to measure the change in indoor temperature and humidity. The building size is 4 m × 3 m × 2.7 m, and the wall thickness is 370 mm. There is an outer door with a size of 2.0 m × 0.9 m and a single glass window with a size of 1.2 m × 1.0 m. There is no heat and humidity source in the room. The general situation of the building and the placement of temperature and humidity sensors are shown in Figure 5. The measurement data for one week in January were selected for model validation.

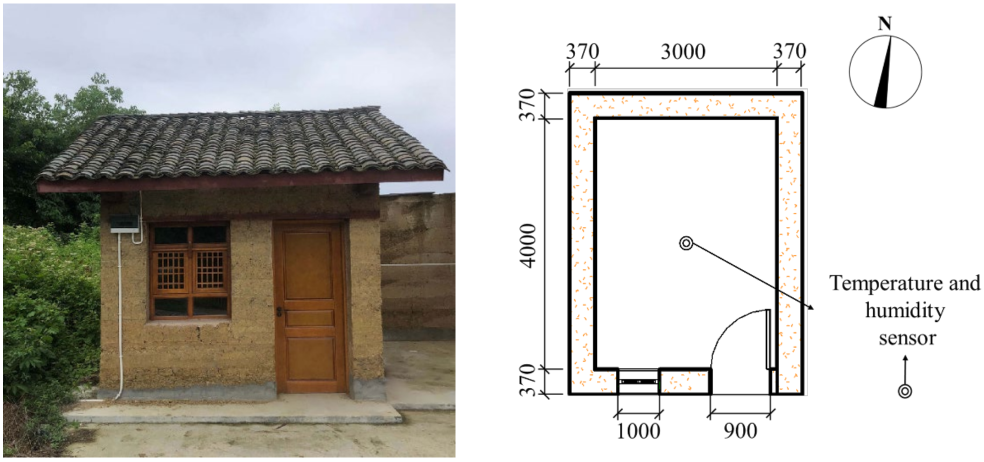

(**a**) (**b**)

Figure 5. The general situation of the rammed earth building (**a**) and the placement of temperature and humidity sensors (**b**).

The comparison between the simulation results and measurement data is shown in Figure 6. The maximum relative errors in temperature and relative humidity were 11.43% and 5.33%, respectively, with an average relative error of 7.74% and 3.13%, respectively. It indicates that the numerical model is in good agreement with the measurement results.

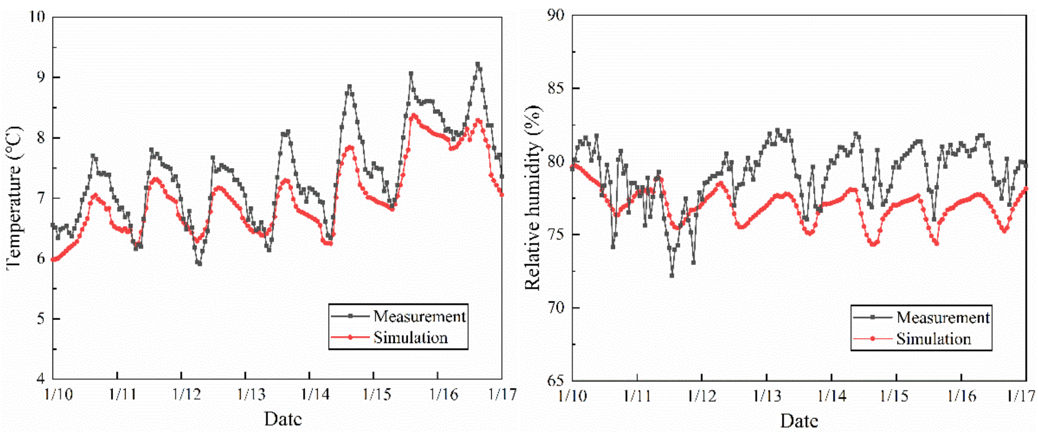

(**a**) (**b**)

Figure 6. Comparison of simulated temperature (**a**) and RH (**b**) with measurement data.

4. Simulation of Heat and Moisture Transfer

In this study, a variety of working conditions were simulated and analyzed using the rammed earth wall in Northwest Sichuan as an example. The PDE module of COMSOL software was used to solve the heat and moisture transfer model and the indoor air heat and moisture balance equations. The uniform mesh grid was adopted in the simulation and the size was 0.01 mm. The thermal conductivity and water vapor permeability of earth materials use the functions fitted in the previous section and the constants, respectively. The constant values of the two coefficients are the integral average value of their functions in the range of 0–100% relative humidity. The constant value of thermal conductivity was 0.598 W/mK, and that of water vapor permeability was 1.341×10^{-11} kg/s·Pa.

4.1. Steady Boundary

To study the influence of material hygrothermal parameters on the heat and moisture transfer of the rammed earth walls under steady boundary conditions, a 370-mm-thick rammed earth wall (Figure 7) was used as the object of study, and its heat and moisture transfer was simulated and calculated. It was assumed that the outdoor temperature and humidity were 35 °C and 90%, respectively, and the indoor was 20 °C and 50%, respectively. The initial state inside of the wall was the same as the indoors, and the calculated duration was 600 h.

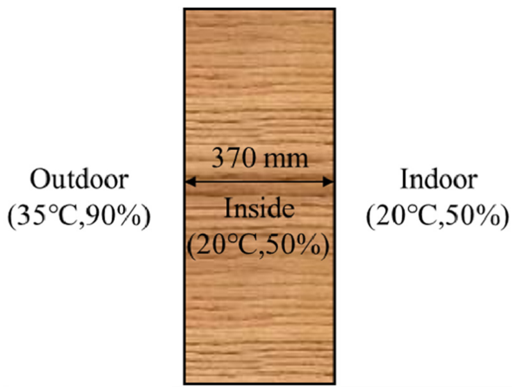

Figure 7. Configurations of the rammed earth wall.

The characteristics of temperature and heat flux variations on the internal surface of the rammed earth wall under the two conditions are shown in Figures 8–10.

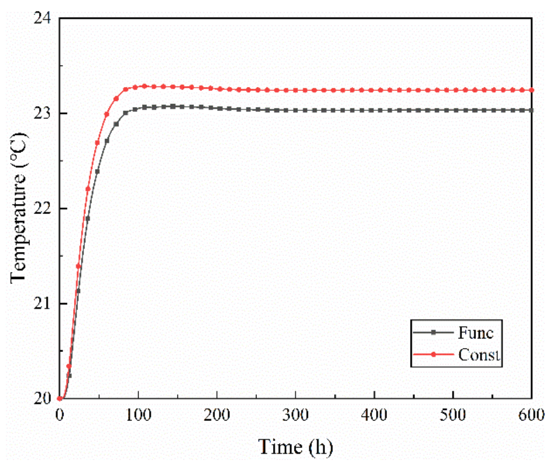

Figure 8. Temperature variation on the internal surface of the wall.

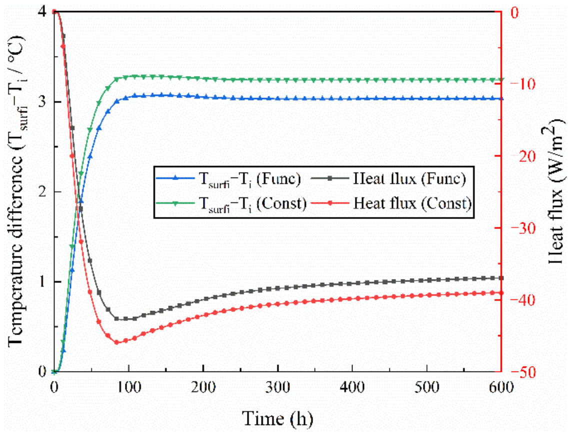

Figure 9. Heat flux and T_{surfi}-T_i variation on the internal surface of the wall.

According to Figures 8 and 9, the negative values of heat flux indicate that the rammed earth wall released heat. T_{surfi}-T_i indicates the temperature difference between the internal surface of the wall and the indoor air. The internal surface of the wall released heat at a higher rate during the initial 85 h, with the heat flux and temperature rising faster and stabilizing after 85 h. The heat flux and temperature on the internal surface under constant conditions were always higher than those under functional conditions. However, the temperature difference was small, and the difference gradually increased and then began to stabilize. The average heat flux and temperature differences were 2.37 W/m^2 and 0.21 °C, respectively, with an average relative error of 8.42% and 0.93%. The reasons are as follows: the indoor air temperature and relative humidity were low, and the internal surface of the wall releases moisture and heat. The thermal conductivity of the constant condition was greater than that of the function condition, and the heat release rate under the constant condition was greater. Meanwhile, the moisture transfer under constant conditions was greater than that under functional conditions. The latent heat of phase change under constant conditions was correspondingly greater, and the temperature rise caused by the latent heat of phase change was higher (shown in Figure 10), which causes the difference in heat flux and temperature increase. As the temperature inside the wall increases, the heat release rate begins to decrease and becomes stable. The heat flux and temperature begin to stabilize and the difference between the two conditions is stable.

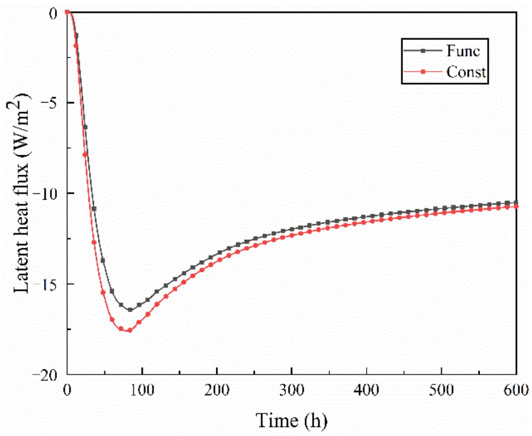

Figure 10. Latent heat flux variation on the internal surface of the wall.

As shown in Figure 10, the internal surface of the wall released heat at a higher rate during the initial 85 h, with the latent heat flux rising faster and starting to decrease after 85 h. The latent heat flux on the internal surface under constant conditions was always greater than that under functional conditions, and the difference gradually increased and then began to stabilize. The average latent heat flux difference was 0.50 W/m^2, with an average relative error of 6.07%. The reasons are as follows: the indoor air relative humidity was low, and the internal surface of the wall releases moisture. The water vapor permeability of the constant condition was greater than that of the functional condition, and the moisture release rate under constant conditions was greater. Meanwhile, the thermal conductivity under constant conditions was greater than that under functional conditions, which increases the difference in latent heat flux. As the moisture content inside the wall increases, the moisture release rate begins to decrease, as well as the moisture flux. The latent heat flux begins to decrease and the difference between the two conditions was stable.

4.2. Period Boundary

To investigate the influence of material hygrothermal parameters on the heat and moisture transfer of rammed earth walls under the diurnal variation in the indoor and outdoor temperatures and humidity, a 370-mm-thick rammed earth wall was used as the object of study. The heat and moisture transfer of the wall were simulated and calculated. The calculation conditions [36] are listed in Table 4.

Table 4. Indoor and outdoor temperature and humidity during different working conditions.

	Case 1	Case 2
Outdoor temperature	$T_e(t) = 303.15 + 3\cos\left(\frac{\pi t}{12} - 161\right)$	$T_e(t) = 303.15 + 3\cos\left(\frac{\pi t}{12} - 161\right)$
Indoor temperature	$T_i(t) = 299.15 + 2.5\cos\left(\frac{\pi t}{12} - 161\right)$	$T_i(t) = 299.15 + 2.5\cos\left(\frac{\pi t}{12} - 161\right)$
Outdoor relative humidity	$\varphi_e(t) = 0.7 - 0.1\cos\left(\frac{\pi t}{12} + 2.6\right)$	$\varphi_e(t) = 0.4 - 0.1\cos\left(\frac{\pi t}{12} + 2.6\right)$
Indoor relative humidity	$\varphi_i(t) = 0.7 - 0.05\cos\left(\frac{\pi t}{12} + 2.6\right)$	$\varphi_i(t) = 0.4 - 0.05\cos\left(\frac{\pi t}{12} + 2.6\right)$

Cases 1 and 2, with different working conditions, represent the periodic variations in temperature and humidity in humid and dry areas in summer, respectively. The initial state inside the wall was the same as that on the internal of the wall, and the calculated duration was 168 h. To eliminate the influence of the initial value on the calculation results, the calculation results of the latter 48 h were analyzed.

As shown in Figure 11, the temperature of the internal surface of the wall varies periodically with the indoor and outdoor temperature and humidity, and the temperature difference between the two conditions is small. In Case 1, the average temperature was 26.76 °C and 26.86 °C under the function and constant conditions, respectively, with a maximum temperature difference of 0.1 °C. In Case 2, the average temperature was 26.88 °C and 26.93 °C under the function and constant conditions, respectively, with a maximum temperature difference of 0.06 °C.

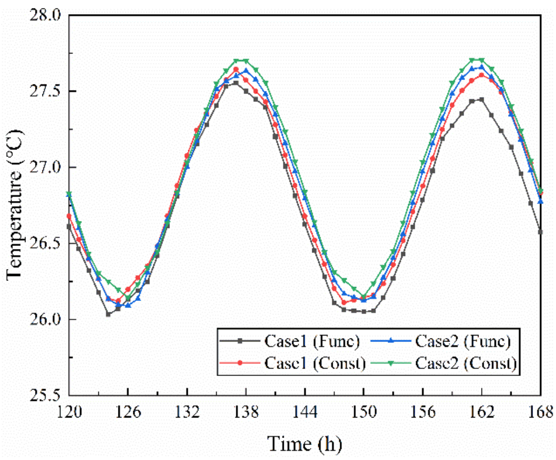

Figure 11. Temperature variation on the internal surface of the wall.

As shown in Figure 12, the negative values of heat flux indicate that the rammed earth wall releases heat, while the positive values indicate that heat is absorbed. In Case 1, the heat flux was 922.15 W/m^2 under constant conditions, which is 4.65% higher than 881.14 W/m^2 under functional conditions. In Case 2, the heat flux was 667.10 W/m^2 under constant conditions, which is 2.02% higher than 653.88 W/m^2 under functional conditions.

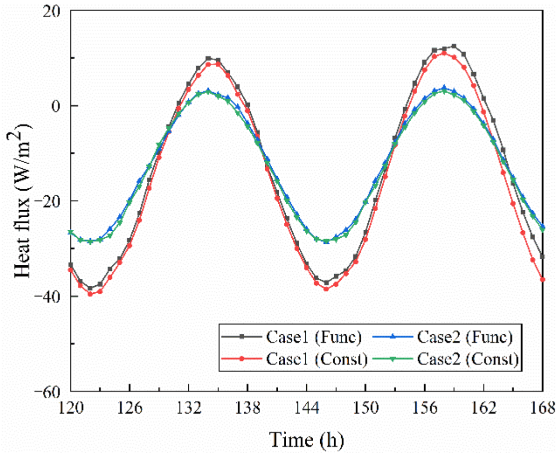

Figure 12. Heat flux variation on the internal surface of the wall.

Figure 13 shows the variation of the latent heat flux on the internal surface of the wall. In Case 1, the latent heat flux was 365.87 W/m^2 under constant conditions, which is 9.93% higher than 332.83 W/m^2 under functional conditions. In Case 2, the latent heat flux was 216.15 W/m^2 under constant conditions, which is 0.30% lower than 216.79 W/m^2 under functional conditions.

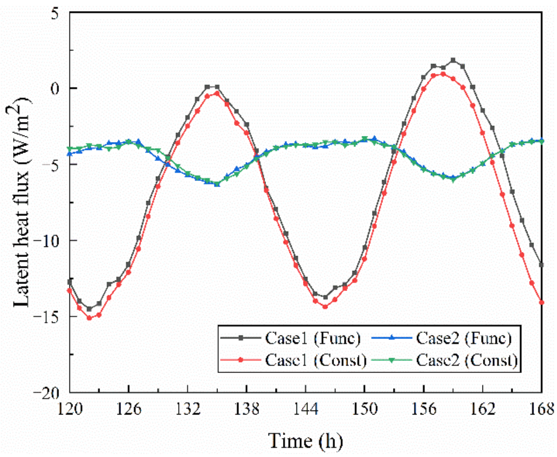

Figure 13. Latent heat flux variation on the internal surface of the wall.

The above results indicate that the non-constant hygrothermal parameters have little influence on the internal surface temperature of the rammed walls but have a great influence on the heat transfer. The difference in heat transfer between the two conditions is more obvious in high temperature and high humidity conditions.

4.3. Mianyang Climate Boundary

The results show that whether the hygrothermal parameters are constant or not makes a difference to the heat flux on the internal surfaces of the walls. For ordinary buildings, the indoor temperature and humidity are mainly influenced by the heat and moisture fluxes on the internal surfaces of the walls. Therefore, to investigate the influence of hygrothermal parameters of the wall material on the indoor heat and moisture environment, this section simulates the changes in rammed earth building indoor temperature and humidity, as well as the heat transfer of the internal surfaces of the wall under the climatic conditions in Mianyang City. The hygrothermal parameters of the wall are taken as functions and constants, respectively.

The outdoor meteorological parameters were obtained from typical meteorological year data for Mianyang City, and the initial temperature and humidity conditions inside the walls were consistent with the climate. The size of the room was 4 m × 3 m × 3 m, and the thickness of the wall was 370 mm. The number of air changes in the room was 1 ACH, and there were no sources of heat or humidity in the room. The air penetrating the room through the gaps in the windows and doors was ignored, and the effect of solar radiation on the walls in all orientations was considered. It was assumed that the floor and roof were waterproofed and insulated and the air in the room was well mixed. The calculated duration was 365 d and the results were recorded for one week in January and one week in July to analyze the changes in the indoor temperature and humidity. Finally, the differences in heat transfer throughout the year were analyzed.

As shown in Figures 14 and 15, the difference in temperature and humidity between the two conditions was insignificant. During winter, the indoor average temperature was 6.29 °C and 6.32 °C under the function and constant conditions, respectively, with the maximum temperature difference and maximum relative humidity difference of 0.33 °C and 1.02%. During summer, the indoor average temperature was 26.77 °C and 26.98 °C under the function and constant conditions, respectively, with the maximum temperature difference and maximum relative humidity difference of 0.46 °C and 1.51%.

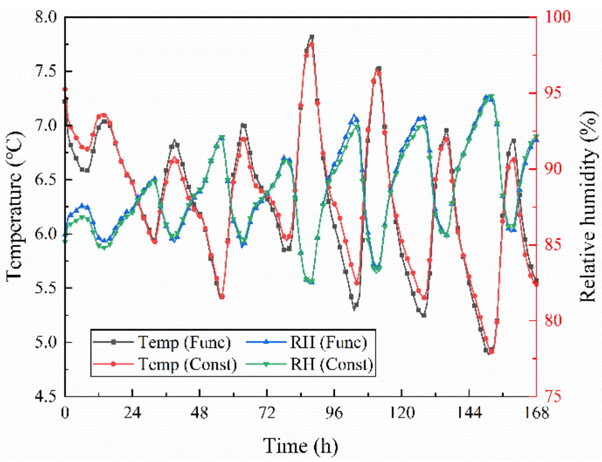

Figure 14. Variation of indoor temperature and humidity in January.

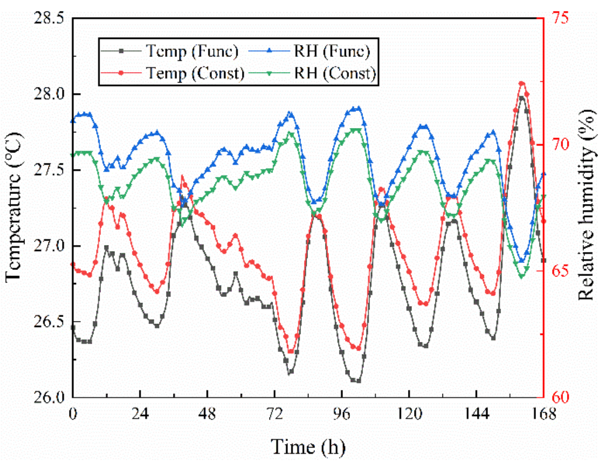

Figure 15. Variation of indoor temperature and humidity in July.

To analyze the influence of the two conditions on the heat transfer to the wall, the heat transfer for the entire year was calculated, as shown in Figure 16. The heat transfer at a given time can be calculated as

$$Q_i = \int_{t_1}^{t_2} \left[h_i \left(T_i - T_{surfi} \right) + h_{lv} g_{n,i} \right] \tag{14}$$

where Q_i is the heat transfer from the internal surface of the wall (J/m^2) and t is the time (s).

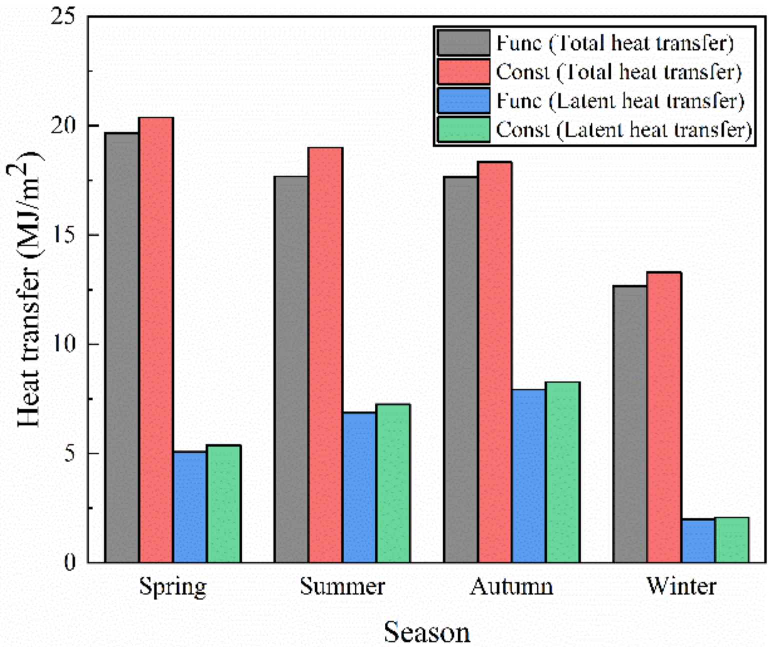

Figure 16. Heat transfer for the entire year.

As shown in Figure 16, the largest difference in heat transfer was 1.33 MJ/m^2 in summer, and the heat transfer under constant conditions was 7.52% higher than that under functional conditions. Meanwhile, the largest difference in latent heat transfer was 0.31 MJ/m^2 in spring, and the latent heat transfer under constant conditions was 6.11% higher than that under functional conditions. In summer, higher outdoor ambient temperature and large temperature difference between indoor and outdoor make a large difference in heat transfer between the two conditions. In spring, higher outdoor ambient humidity and large humidity differences between indoor and outdoor make a large difference in moisture transfer between the two conditions, resulting in large latent heat transfer difference. During the whole year, the heat transfer was 71.03 MJ/m^2 under constant conditions, which is 4.97% higher than 67.67 MJ/m^2 under functional conditions. The latent heat transfer was 22.98 MJ/m^2 under constant conditions, which is 5.03% higher than 21.88 MJ/m^2 under functional conditions. The above results indicate that there is a significant difference in heat transfer on the internal surface between the two conditions in hot and humid areas.

5. Conclusions

In this study, the functional relationship between the thermal conductivity, water vapor permeability, and humidity of earth materials from Northwestern Sichuan was obtained through experiments. A non-stationary model of the heat and moisture transfer in rammed earth walls and indoor air was developed and validated. The function curves and constants of the two coefficients were substituted into the numerical model and solved using COMSOL Multiphysics software. The differences in the heat and moisture transfer of the wall under different working conditions were analyzed when the material hygrothermal parameters were regarded as the functions and constants. The influence of the material hygrothermal parameters on the heat and moisture transfer of the wall was studied and investigated. The following conclusions were drawn:

1. The thermal conductivity of the earth materials from Northwest Sichuan is linearly related to moisture content, with R^2 being greater than 0.98. The water vapor permeability has a small variation in the 0–60% relative humidity range and increases exponentially above 60%.
2. A numerical model with temperature and humidity as driving potential was established. The measured data of the rammed earth building are in good agreement with the simulation results under the same conditions.
3. At a steady boundary, when the moisture content of the rammed earth wall was low, the thermal conductivity and water vapor permeability under the constant condition were higher than that under the function condition, making the temperature and the heat flux on the internal surface of the wall under the constant condition greater. Among them, the average relative error of internal surface temperature was 0.93%, which is small. The average relative error of heat flux and latent heat flux was 8.42% and 6.07%, respectively, which shows a large difference.
4. Under the periodic boundary, the internal surface temperature of the rammed earth wall shows a small difference between the two conditions. The average temperature difference of the internal surface was less than 0.1 °C in wet and dry conditions in summer. The heat flux on the internal surface under constant conditions was 4.65% higher than that under functional conditions, and the latent heat flux on the internal surface under constant conditions was 9.93% higher than that under function conditions in the humid summer condition. In the dry summer conditions, the figures were 2.02% and −0.30%. The heat transfer difference between the two conditions is more obvious in high temperature and high humidity conditions.
5. Under the climate boundary of Mianyang City, the rammed earth building indoor air temperature and humidity in summer and winter were similar under the two conditions. The largest difference in heat transfer on the internal surface was in summer, and under constant conditions was 7.52% higher than that under functional conditions. Meanwhile, the largest difference in latent heat transfer on the internal surface was in spring, and under constant conditions was 6.11% higher than that under functional conditions. Throughout the whole year, the heat flux under constant conditions was 4.97% higher than that under functional conditions, and the latent heat flux under constant conditions was 5.03% higher than that under functional conditions. There is a significant difference in heat transfer between the two conditions in hot and humid areas.

Author Contributions: Conceptualization, J.T. and B.J.; Data curation, J.L.; Supervision, B.J.; Validation, J.L.; Visualization, L.W.; Writing—original draft, J.T.; Writing—review & editing, L.W. All authors have read and agreed to the published version of the manuscript.

Funding: This research was funded by the National Natural Science Foundation of China, grant number 52078439.

Institutional Review Board Statement: Not applicable.

Informed Consent Statement: Not applicable.

Data Availability Statement: Data is contained within the article.

Conflicts of Interest: The authors declare no conflict of interest.

Nomenclature

w	moisture content (kg/m^3)
g	density of moisture flux (kg/m^{2}s)
L	thickness of specimen (m)
m	mass of specimen (kg)
A	superficial area of the specimen (m^2)
R	radius of the specimen (m)
T	temperature (K)
K_l	liquid water permeability (s)
P_v	partial water vapor pressure (Pa)
P_{sat}	partial pressure of saturated vapor (Pa)
R_D	gas constant of water vapor (J/kgK)
$c_{p,m}$	specific heat capacity of dry material (J/kgK)
$c_{p,l}$	specific heat capacity of liquid water (J/kgK)
$c_{p,a}$	specific heat capacity of air (J/kgK)
h_{lv}	latent heat of water phase change (J/kg)
$g_{n,i}$	moisture flux through the internal surface (kg/m^{2}s)
$g_{n,e}$	moisture flux through the external surface (kg/m^{2}s)
$q_{n,i}$	heat flux through the internal surface (W)
$q_{n,e}$	heat flux through the external surface (W)
h	convective heat transfer coefficient (W/m^{2}K)
h_i	convective heat transfer coefficient of internal surface (W/m^{2}K)
h_e	convective heat transfer coefficient of external surface (W/m^{2}K)
$P_{sat,i}$	indoor partial pressure of saturated vapor (Pa)
$P_{sat,e}$	outdoor partial pressure of saturated vapor (Pa)
$P_{sat,surfi}$	partial pressure of saturated vapor on the internal surface (Pa)
$P_{sat,surfe}$	partial pressure of saturated vapor on the external surface (Pa)
T_i	indoor temperature (K)
T_e	outdoor temperature (K)
T_{surfi}	the temperature on the internal surface (K)
T_{surfe}	the temperature on the external surface (K)
q_{solar}	solar radiation (W/m^2)
V	volume of structure (m^3)
Q	heat transfer (J/m^2)
R^2	goodness of fit
Greek symbols	
α	solar absorptivity of the external surface
ρ_a	density of air (kg/m^3)
ρ_l	density of liquid water (kg/m^3)
ρ_m	density of building materials (kg/m^3)
δ_p	water vapor permeability (kg/m·s·Pa)
ξ	sorption capacity (kg/m^3)
λ	thermal conductivity (W/mK)
β	moisture exchange transfer coefficient (m/s)
β_i	moisture exchange transfer coefficient of internal surface (m/s)
β_e	moisture exchange transfer coefficient of external surface (m/s)
φ	relative humidity (%)
φ_i	indoor relative humidity (%)
φ_e	outdoor relative humidity (%)
φ_{surfi}	relative humidity of internal surface (%)
φ_{surfe}	relative humidity of external surface (%)

References

1. Guo, Y.-Y. Revisiting the building energy consumption in China: Insights from a large-scale national survey. *Energy Sustain. Dev.* **2022**, *68*, 76–93. [CrossRef]
2. Ness, D.A.; Xing, K. Toward a Resource-Efficient Built Environment: A Literature Review and Conceptual Model. *J. Ind. Ecol.* **2017**, *21*, 572–592. [CrossRef]

3. Cagnon, H.; Aubert, J.E.; Coutand, M.; Magniont, C. Hygrothermal properties of earth bricks. *Energy Build.* **2014**, *80*, 208–217. [CrossRef]
4. Touré, P.; Sambou, V.; Faye, M.; Thiam, A.; Adj, M.; Azilinon, D. Mechanical and hygrothermal properties of compressed stabilized earth bricks (CSEB). *J. Build. Eng.* **2017**, *13*, 266–271. [CrossRef]
5. Brambilla, A.; Jusselme, T. Preventing overheating in offices through thermal inertial properties of compressed earth bricks: A study on a real scale prototype. *Energy Build.* **2017**, *156*, 281–292. [CrossRef]
6. Liuzzi, S.; Hall, M.R.; Stefanizzi, P.; Casey, S.P. Hygrothermal behaviour and relative humidity buffering of unfired and hydrated lime-stabilised clay composites in a Mediterranean climate. *Build. Environ.* **2013**, *61*, 82–92. [CrossRef]
7. Hall, M.; Allinson, D. Analysis of the hygrothermal functional properties of stabilised rammed earth materials. *Build. Environ.* **2009**, *44*, 1935–1942. [CrossRef]
8. Sabbà, M.F.; Tesoro, M.; Falcicchio, C.; Foti, D. Rammed Earth with Straw Fibers and Earth Mortar: Mix Design and Mechanical Characteristics Determination. *Fibers* **2021**, *9*, 30. [CrossRef]
9. Yi, H. Rapid thermal conductivity measurement with a hot disk sensor. *Thermochim. Acta* **2005**, *436*, 122–129.
10. Nikiforova, T.; Savytskyi, M.; Limam, K.; Bosschaerts, W.; Belarbi, R. Methods and Results of Experimental Researches of Thermal Conductivity of Soils. *Energy Procedia* **2013**, *42*, 775–783. [CrossRef]
11. Huangfu, H.; Jin, H. Experimental study of the effect of moisture content on the thermal conductivity of earth commonly used in engineering. *Water Resour. Power* **2015**, *33*, 122–124.
12. Zheng, Q.; Jin, H.; Liu, H.; Zhang, C.; Niu, K. Effect of porosity and water content on the thermal conductivity of sandy earth samples. *Water Resour. Power* **2015**, *33*, 125–128.
13. Mukhopadhyaya, P.; Kumaran, M.K.; Lackey, J. Use of the modified cup method to determine temperature dependency of water vapor transmission properties of building materials. *J. Test. Eval.* **2005**, *33*, 316–322.
14. Li, K.; Zhang, X.; Han, X.; Zhu, D. Experimental study of the water vapour permeability of building materials. *J. Build. Mater.* **2009**, *12*, 284–287.
15. Bai, W. *Structural Renewal of Dwellings and Sustainable Use of Natural Building Materials in Yunnan*; Tsinghua University: Beijing, China, 2009.
16. Korjenic; Sinan; Ashour; Taha; Wei; Azra. Thermal conductivity of unfired earth bricks reinforced by agricultural wastes with cement and gypsum. *Energy Build.* **2015**, *104*, 139–146. [CrossRef]
17. Mansour, M.B.; Jelidi, A.; Cherif, A.S.; Jabrallah, S.B. Optimizing thermal and mechanical performance of compressed earth blocks (CEB). *Constr. Build. Mater.* **2016**, *104*, 44–51. [CrossRef]
18. Giada, G.; Caponetto, R.; Nocera, F. Hygrothermal Properties of Raw Earth Materials: A Literature Review. *Sustainability* **2019**, *11*, 5342. [CrossRef]
19. Chu, S.S.; Fang, T.H.; Chang, W.J. Modelling of coupled heat and moisture transfer in porous construction materials. *Math. Comput. Model.* **2009**, *50*, 1195–1204. [CrossRef]
20. Santos, G.; Mendes, N. Heat, air and moisture transfer through hollow porous blocks. *Int. J. Heat Mass. Transf.* **2009**, *52*, 2390–2398. [CrossRef]
21. Chow, T.T.; Fong, K.F.; Givoni, B.; Lin, Z.; Chan, A. Thermal sensation of Hong Kong people with increased air speed, temperature and humidity in air-conditioned environment. *Build. Environ.* **2010**, *45*, 2177–2183. [CrossRef]
22. Pei, Q.Q.; Chen, Z.K. An Experimental Study on Isothermal Moisture Absorption and Desorption Processes of Some Common used Building Materials. *J. Hunan Univ.* **1999**, *26*, 96–99.
23. van Schijndel, A.W.M. Multiphysics modeling of building physical constructions. *Build. Simul.* **2011**, *4*, 49–60. [CrossRef]
24. Liu, D.; Zhao, H.; Liu, X.; He, Q. Testing the thermal conductivity of earth at different moisture contents and the effect on building energy consumption. *J. Civ. Environ. Eng.* **2017**, *39*, 20–25.
25. *SL237-1999*; Specification of Soil Test. Institute, N.H.R.: Beijing, China, 1999.
26. Shang, J. Optimisation of Ecological Building Material Systems for Traditional Rammed Earth Dwellings. Ph.D. Thesis, Xi'an University of Architecture and Technology, Xi'an, China, 2005.
27. *BS EN ISO 12572*; Hygrothermal Performance of Building Materials and Products—Determination of Water Vapour Transmission Properties—Cup Method. British Standards Institution: London, UK, 2016.
28. Dean, J.A. *Lange's Handbook of Chemistry*, 15th ed.; McGraw-Hill, Inc.: St. Louis, MO, USA, 1999.
29. Galbraith, G.H.; McLean, R.C.; Guo, J. Moisture permeability data: Mathematical presentation. *Build. Serv. Eng. Res. Technol.* **1998**, *19*, 31–36. [CrossRef]
30. Liang, J.; Tan, J.; Jiang, B. Thermal and humid environment of rammed-earth dwellings in Northwest Sichuan. *Indoor Built Environ.* **2022**, *31*, 645–656. [CrossRef]
31. Bear, J. Modelling Transport Phenomena in Porous Media. In *Convective Heat and Mass Transfer in Porous Media*; Kakaç, S., Kilkiş, B., Kulacki, F.A., Arinç, F., Eds.; Springer Netherlands: Dordrecht, The Netherlands, 1991; pp. 7–69.
32. Kast, D.; Jokisch, F. Considerations regarding the development of sorption isotherms and the sorption kinetics in porous solids. *Chem. Ing. Technol.* **1972**, *44*, 556–563. [CrossRef]
33. Liu, X.; Chen, Y.; Ge, H.; Fazio, P.; Chen, G. Numerical investigation for thermal performance of exterior walls of residential buildings with moisture transfer in hot summer and cold winter zone of China. *Energy Build.* **2015**, *93*, 259–268. [CrossRef]

34. Liu, Y.; Wang, Y.; Wang, D.; Liu, J. Effect of moisture transfer on internal surface temperature. *Energy Build.* **2013**, *60*, 83–91. [CrossRef]
35. Yan, Z. *Study of Indoor Heat and Moisture Environments in Rammed Earth Buildings*; Xi'an University of Architecture and Technology: Xi'an, China, 2003.
36. Wang, L. *Study of Thermal Processes in Envelope Structures under the Effect of Periodic Double Fluctuations*; Xi'an University of Architecture and Technology: Xi'an, China, 2010.